


# Enhanced photothermal performance of dielectric silicon attached with multiple plasmonic gold nanoparticles

Xiangyu Tong(佟翔宇), Ning Chen(陈宁), Xiaowen Chen(陈晓文), Bin Zhang(张斌), and Xiaohu Wu(吴小虎)
**Citation:**Chin. Phys. B, 2025, 34 (**8**): 087803. DOI: 10.1088/1674-1056/add90b
http://cpb.iphy.ac.cn; http://iopscience.iop.org/cpb

**What follows is a list of articles you may be interested in**

---

## Strong field ionization of molecules on the surface of nanosystems

Qiwen Qu(曲棋文), Fenghao Sun(孙烽豪), Jiawei Wang(王佳伟), Jian Gao(高健), Hui Li(李辉), and Jian Wu(吴健)
Chin. Phys. B, 2024, 33 (**4**): 047803. DOI: 10.1088/1674-1056/ad2509

## Quantitative evaluation of LAL productivity of colloidal nanomaterials: Which laser pulse width is more productive, ergonomic, and economic?

Alena Nastulyavichus, Nikita Smirnov, and Sergey Kudryashov
Chin. Phys. B, 2022, 31 (**7**): 077803. DOI: 10.1088/1674-1056/ac5602

## Strong near-field couplings of anapole modes and formation of higher-order electromagnetic modes in stacked all-dielectric nanodisks

Bin Liu(刘彬), Ma-Long Hu(胡马龙), Yi-Wen Zhang(章艺文), Yue You(游悦), Zhao-Guo Liang(梁钊国), Xiao-Niu Peng(彭小牛), and Zhong-Jian Yang(杨中见)
Chin. Phys. B, 2022, 31 (**5**): 057802. DOI: 10.1088/1674-1056/ac3bac

## Improving the performance of a GaAs nanowire photodetector using surface plasmon polaritons

Xiaotian Zhu(朱笑天), Bingheng Meng(孟兵恒), Dengkui Wang(王登魁), Xue Chen(陈雪), Lei Liao(廖蕾), Mingming Jiang(姜明明), and Zhipeng Wei(魏志鹏)
Chin. Phys. B, 2022, 31 (**4**): 047801. DOI: 10.1088/1674-1056/ac1e15

## Effects of thickness & shape on localized surface plasmon resonance of sexfoil nanoparticles

Yan Chen(陈艳), Xianchao Liu(刘贤超), Weidong Chen(陈卫东), Zhengwei Xie(谢征微), Yuerong Huang(黄跃容), Ling Li(李玲)
Chin. Phys. B, 2017, 26 (**1**): 017807. DOI: 10.1088/1674-1056/26/1/017807

---

**SPECIAL TOPIC — Artificial intelligence and smart materials innovation: From fundamentals to applications**

# Enhanced photothermal performance of dielectric silicon attached with multiple plasmonic gold nanoparticles

Xiangyu Tong(佟翔宇)[1], Ning Chen(陈宁)[2], Xiaowen Chen(陈晓文)[1], Bin Zhang(张斌)[1,†], and Xiaohu Wu(吴小虎)[3,‡]

[1] *College of Electromechanical Engineering, Qingdao University of Science and Technology, Qingdao* 266061, *China*

[2] *Medical Science and Technology Innovation Center, Shandong First Medical University & Shandong Academy of Medical Sciences, Jinan* 250100, *China*

[3] *Thermal Science Research Center, Shandong Institute of Advanced Technology, Jinan* 250100, *China*

(Received 7 April 2025; revised manuscript received 13 May 2025; accepted manuscript online 15 May 2025)

The photothermal properties of dielectric materials at the nanoscale have garnered significant attention, especially in fields such as optical heating, photothermal therapy, and solar utilization. However, although dielectric materials can concentrate and manipulate light at the nanoscale, they cannot provide sufficient photothermal efficiency in a direct absorption solar collector. Combining plasmonic metal nanoparticles with dielectric nanostructures enables the fabrication of hybrid nanomaterials with excellent photothermal performance. This study presents a novel approach involving uniformly adhering plasmonic gold nanoparticles onto dielectric silicon nanoparticles to enhance the absorption peak, leading to a substantial enhancement of photothermal conversion efficiency. The results demonstrate that the absorption peak of silicon-gold hybrid nanoparticles exceeds that of pure silicon nanoparticles, achieving a 38% increase in photothermal conversion efficiency within a 10 ppm aqueous solution under a 20 mm optical path. The coupling of localized surface plasmon resonance and quadrupole resonance effects enhances the electric field, causing a temperature rise in both the hybrid nanoparticles and the surrounding aqueous solution. Nanostructural modulation studies reveal that the photothermal efficiency of silicon-gold hybrid nanoparticles is positively correlated with gold nanoparticle size but negatively correlated with silicon nanoparticle size. Combining multiple plasmonic nanoparticles with dielectric materials can effectively enhance photothermal performance and hold great application potential in direct absorption solar collectors and solar thermal utilization.

**Keywords:** silicon–gold hybrid nanoparticles, localized surface plasmon resonance, dielectric nanomaterial, solar utilization

**PACS:** 78.67.Bf, 73.20.Mf, 77.84.–s, 88.40.–j

**DOI:** 10.1088/1674-1056/add90b **CSTR:** 32038.14.CPB.add90b

## 1. Introduction

With the development of nanotechnology, dielectric nanoparticles with distinctive optical properties have attracted widespread attention owing to their ability to induce electrical and magnetic resonances when exposed to light.[1,2] Additionally, dielectric nanomaterials such as silicon have received notable attention for their ability to enhance resonant fields and maintain thermal stability, which positions them as promising candidates for various applications including optical heating,[3–5] photothermal therapy,[6,7] and solar utilization.[8–10] Silicon, regarded as a pivotal nano-dielectric material, holds significant research potential and application opportunities. However, the limited photothermal conversion efficiency observed in silicon nanoparticle suspensions poses challenges to its advancement, necessitating further investigation.[11]

Due to the strong Mie resonance that occurs within the visible spectrum, silicon dielectric nanoparticles exhibit significant optical characteristics. Through structural design and material selection, Mie resonances or plasmonic resonances can induce Fano resonances, thereby affecting the optical properties of nanostructures.[12–14] Zograf *et al.*[15] have shown experimentally and theoretically that spherical silicon nanoparticles with a magnetic quadrupole Mie resonance are able to convert light energy into heat with an efficiency that is four times greater than that of comparable spherical gold nanoparticles when subjected to identical heating conditions. Amjad *et al.*[16] explored the properties of various nanofluids containing Si, $Al_2O_3$-Y, Fe, Zn, Cu, and Ag nanofluids and found that the photothermal conversion efficiency of Si is low, while metal nanoparticles with localized surface plasmon resonance (LSPR) have higher photothermal conversion efficiency. In metal nanoparticles, LSPR occurs when the overall vibrational frequency of free electrons matches the frequency of incident light, which is closely related to the size, shape, composition, structure, and other factors.[17–20] Chen *et al.*[21] investigated the photothermal response characteristics of silver and gold plasmonic nanomaterials, and discovered that the

†Corresponding author. E-mail: zb-sh@163.com

‡Corresponding author. E-mail: wuxiaohu@pku.edu.cn

© 2025 Chinese Physical Society and IOP Publishing Ltd. All rights, including for text and data mining, AI training, and similar technologies, are reserved.

triangular pyramidal nanostructures enhance the surface plasmon resonance associated with silver and gold specifically within the near-infrared spectrum. Zou *et al.*[22] presented a nanorod consisting of broadband absorbing C and a plasmonic resonance Cu. Compared with nanoparticles alone, this innovative design enables C–Cu core–shell nanorods to enhance resonance absorption peaks.

Therefore, by merging the essential benefits of various nanoparticles, the creation of hybrid nanoparticles can lead to the development of nanomaterials that possess outstanding optical characteristics, opening up new possibilities for the fabrication of advanced materials with tailored optical properties for a wide range of applications.[23–25] Scholars have utilized numerical methods and experiments to study hybrid nanoparticles, Zhou *et al.*[26] utilized the finite element method to model the two-dimensional structure of a silicon nanowire that was coated with metal nanoparticles, specifically Au, Ag, and Al, in air. Ge *et al.*[27] employed a three-dimensional method to numerically simulate the effects of gold nanoparticle size and silica dielectric layer thickness on the properties of Au/$SiO_2$ nanoparticles. Whereas in the experimental preparation, Gerasimova *et al.*[28] introduced a single-step method utilizing high-throughput laser ablation to fabricate a composite structure consisting of Au nanoparticles and Si nanoparticles. The incorporation of the additional gold component in the hybrid Si–Au nanoparticles resulted in a broadening of the resonance, which facilitated effective optical heating and nano thermometry applications. Gurbatov *et al.*[29] synthesized Au@Si nanocomposites with unique compositions and morphologies in one step and found effective absorption of incident radiation in a wide spectral range for nano spectroscopy and sensing applications. In addition, such composite structures can also be fabricated using techniques such as seed-mediated growth, photoreduction, chemical deposition, and self-assembly. The interfacial bonding, particle size and distribution control, as well as cost and reproducibility, need to be considered in the practical application process.

The optical and photothermal properties of dielectric, metallic, and hybrid nanoparticles are related to their size and shape.[30–33] Sun *et al.*[34] found that the core-shell composite nanorods improved the absorption efficiency in the visible and near-infrared spectral regions compared to ordinary gold nanorods and the optimal sizes for achieving maximum absorption efficiency were found to be 5 nm, 30 nm, and 60 nm, respectively. Yang *et al.*[35] investigated the core-shell dimensions and the photothermal conversion efficiency of ZrC–Au core–shell nanoparticles at specific parameters in direct absorption solar collectors (DASCs). Core–shell structures are suitable for applications requiring core protection or hierarchical functionalities; however, they often involve high fabrication costs. Conversely, particle-attached structures have garnered significant attention due to their efficient fabrication and compatibility with multiple components. Wu *et al.*[36] synthesized CuSAu hybrid materials that achieved photothermal conversion efficiencies of 67.31% and 32.02% under different laser irradiations. Additionally, simulations indicated that attaching spherical particles to plates significantly enhanced electric field strength and temperature distribution.

Based on the above research, dielectric nanoparticles of Si can effectively convert light into heat; however, their photothermal conversion efficiency is relatively low. Metal nanoparticles of Au can enhance light absorption capabilities owing to their LSPR, but their synthesis is costly. Considering fabrication processes and costs, few studies have applied attached nanostructures to direct absorption solar collectors. In this study, we propose a novel approach to enhance the photothermal conversion efficiency of nanofluids by designing particle attachments that combine the advantages of Si and Au for use in direct absorption solar collectors. Through our analysis, we conducted a comparative examination of the optical parameters and temperature variations associated with both the Si nanoparticles and the Si–Au hybrid nanoparticles. Furthermore, we calculated the photothermal conversion efficiencies across various scenarios to ascertain the performance of these constructed nanoparticle structures. The photothermal conversion mechanism of Si–12Au hybrid nanoparticles has been elucidated through an extensive analysis of the distributions of electric and magnetic fields at the peak of resonance absorption. Furthermore, the research investigated the efficiencies of photothermal conversion in nanofluids containing different sizes of silicon and gold nanoparticles. Ultimately, the findings from this research are expected to provide significant theoretical support for the integration of nanoparticles with both plasmonic and dielectric materials, advancing the field of solar photothermal utilization.

## 2. Models and methods

The geometric model of the proposed Si–Au hybrid nanoparticles is depicted in Fig. 1. The Si sphere has a radius of $R = 60$ nm, and the radius of the Au sphere is $r = 15$ nm. To minimize the effects of incident light direction and polarization on the nanoparticles, twelve Au spheres are uniformly distributed on the surface of the silicon Si sphere. In this configuration, the spacing between the Si and Au cores is set to $R + r$. The wavelength range is 300–1100 nm.

In nanophotonic and photothermal applications, optical parameters are key factors in describing how materials interact with electromagnetic waves. The refractive index serves as a significant characteristic and is typically represented as a complex number. Water is used as the external medium, with a refractive index of 1.33. In nonmagnetic materials, the refractive index $n$ is related to the dielectric constant $\varepsilon$ by the

formula $\varepsilon = n^2$. The refractive indices of Si and Au nanoparticles shown in Fig. 2 are taken from Refs. [37,38]. The thermal characteristics of the materials utilized in the simulation are displayed in Table 1, encompassing key factors such as thermal conductivity, specific heat capacity, and density.

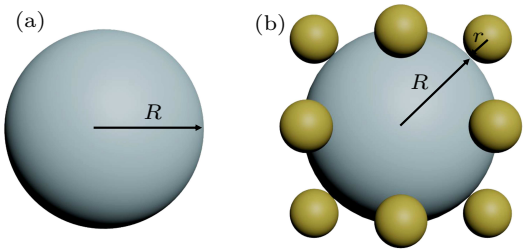



**Fig. 1.** Geometry diagrams of nanoparticles: (a) Si, (b) Si and Au core spacing is $R+r$.

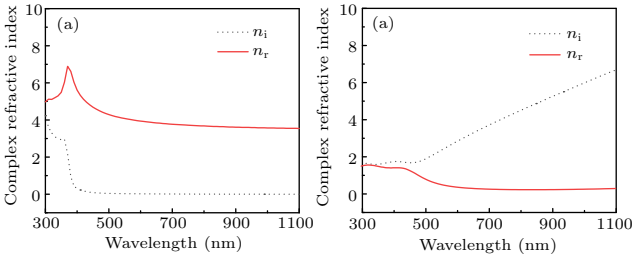



**Fig. 2.** The complex refractive index of (a) Si nanoparticle, (b) Au nanoparticle.

**Table 1.** The thermal properties of Si, Au and water.

| Materials | $\rho$ (kg/m$^3$) | $c$ (J·kg/K) | $k$ (W/(m·K)) |
|---|---|---|---|
| Si | 2330 | 700 | 138 |
| Au | 19300 | 126 | 318 |
| Water | 100 | 4200 | 0.6 |

In this study, we simulated the optical properties of the material using the finite element method (FEM).[39] The simulations were carried out through the wave optics module and the heat transfer module to acquire optical properties such as absorption cross-section, scattering cross-section, and temperature distribution.[40,41] A perfectly matched layer (PML) was added to the external boundary, and surface radiation boundary conditions for thermal convection and radiation to the environment were applied. The initial temperature is set to 293.15 K.

Maxwell's equations are the fundamental equations of electromagnetism. Under steady-state conditions and in frequency domain analysis, they can be simplified to the Helmholtz equation[42]

$$\nabla \times \left(\mu_r^{-1} \nabla \times E\right) - k_0^2 \varepsilon_r E = 0, \tag{1}$$

where $\mu_r$ is the relative permeability, $E$ is the electric field, $k_0 = 2\pi/\lambda$ is the wave number, $\lambda$ is the wavelength, and $\varepsilon_r = (n_r - jn_i)^2$ is the dielectric function. $n_r$ and $n_i$ are the real and imaginary parts of the refractive index, respectively. The dimensionless absorption efficiency ($Q_{abs}$) and scattering efficiency ($Q_{sca}$) are important parameters for the optical properties of nanoparticles[43]

$$Q_{abs} = \frac{C_{abs}}{\sigma}, \tag{2}$$

$$Q_{sca} = \frac{C_{sca}}{\sigma}, \tag{3}$$

where $\sigma$ is the maximum cross-sectional area of the nanoparticle. $C_{abs}$ is the absorption cross-section, and $C_{sca}$ is the scattering cross-section, which are calculated by

$$C_{abs} = \frac{1}{I_{in}} \iiint Q_r \, dV, \tag{4}$$

$$C_{sca} = \frac{1}{I_{in}} \iint (n \cdot S_{sca}) \, dS, \tag{5}$$

where $Q_r$ is the absorbed power density, $V$ is the volume of the nanoparticles, $I_{in}$ is the incident light intensity, which is set to 1 mW/μm$^2$, $n$ is the normal incident vector, $S_{sca}$ is the scattered Poynting vector, representing the energy flow density of the scattered light, and $S$ is the surface area of the nanoparticles.

The absorbed power density can be calculated from Joule heating or dissipated power[44]

$$Q_r = \frac{1}{2} \varepsilon_0 \omega \varepsilon'' |E|^2, \tag{6}$$

where $\varepsilon_0$ is the vacuum dielectric constant, $\omega$ is the incident light frequency, and $\varepsilon''$ is the imaginary part of the dielectric constant of the nanoparticles.

In addition, dispersing nanoparticles in a base fluid is referred to as a nanofluid. The base fluid used in this study is water. The absorption coefficient of the nanofluid can be calculated as

$$k_{\alpha\lambda,nf} = k_{\alpha\lambda,bf} + k_{\alpha\lambda,np} = \frac{4\pi\kappa}{\lambda} + \frac{f_v C_{abs}}{V}, \tag{7}$$

where $k_{\alpha\lambda,nf}$, $k_{\alpha\lambda,bf}$, and $k_{\alpha\lambda,np}$ are the absorption coefficients of the nanofluid, base fluid, and nanoparticles, respectively. $\kappa$ is the absorption index of the base fluid, $\lambda$ is the wavelength of the incident light, and $f_v$ is the volume fraction of the nanoparticles.

The temperature rise of nanofluids requires a combination of solid and convective heat transfer, and the heat transfer equation is given by[45]

$$\rho c \frac{\partial T}{\partial t} + \nabla \cdot (-k \nabla T) = Q, \tag{8}$$

where $\rho$ is the density, $c$ is the specific heat capacity, $k$ is the thermal conductivity, $T$ is the temperature, and $Q$ is the heat source.

The photothermal conversion efficiency ($\eta_{abs}$) of nanofluids refers to the efficiency with which the nanofluid converts light energy into heat energy. It is an important indicator for assessing the performance of nanofluids in absorbing solar radiation and converting it into heat. According to Beer–Lambert's law, the light absorption of nanofluids is closely related to factors such as their concentration, optical path, and

wavelength.[46] The transmissivity and absorbance of nanofluids can be calculated as[47]

$$T_{\mathrm{s}}(\lambda) = \mathrm{e}^{-hk_{\alpha\lambda,\mathrm{nf}}}, \tag{9}$$

$$A(\lambda) = -\log_{10} T_{\mathrm{s}}(\lambda), \tag{10}$$

where $T_{\mathrm{s}}(\lambda)$ is the transmissivity, $A(\lambda)$ represents the absorbance, and $h$ denotes the optical path length.

This provides the relationship between light absorption and propagation in the nanofluid, expressed as

$$I_{\mathrm{abs}}(\lambda) = I_{\mathrm{s}}(\lambda)\left(1 - \mathrm{e}^{-hk_{\alpha\lambda,\mathrm{nf}}}\right), \tag{11}$$

$$\eta_{\mathrm{abs}} = \frac{\int_{0.3\ \mu\mathrm{m}}^{1.1\ \mu\mathrm{m}} I_{\mathrm{abs}}(\lambda)\,\mathrm{d}\lambda}{\int_{0.3\ \mu\mathrm{m}}^{1.1\ \mu\mathrm{m}} I_{\mathrm{s}}(\lambda)\,\mathrm{d}\lambda}, \tag{12}$$

where $I_{\mathrm{abs}}(\lambda)$ is the absorption spectrum, and $I_{\mathrm{s}}(\lambda)$ represents the solar spectrum at AM 1.5.

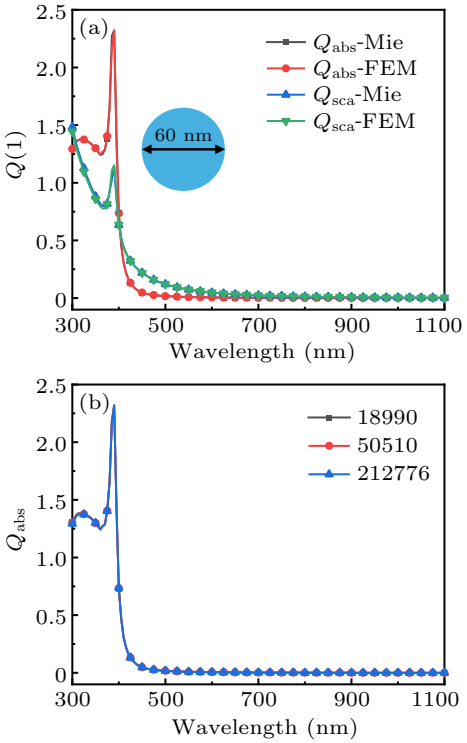



**Fig. 3.** (a) Validation of the model: The outcomes for the Si nanoparticle are computed using FEM and Mie theory. (b) Verification of mesh independence.

The Mie theory serves as a fundamental theoretical framework for analyzing the optical behavior of spherical particles — including metals, semiconductors, and dielectric materials — at the nanoscale.[48] To ensure the reliability and accuracy of our model, we performed a comparative analysis of the optical parameters of Si nanoparticles with a diameter of 60 nm. This was achieved by conducting calculations using both the FEM and Mie theory. The results of this comparison are shown in Fig. 3(a). The calculated absorption and scattering coefficients from both methods exhibit excellent agreement, with a maximum deviation of less than 3%. These findings validate the accuracy of the model adopted in this work, confirming its suitability for simulation purposes.

In FEM, the solution domain is discretized into numerous small and simple subdomains, with a mathematical model constructed for each to approximate the physical behavior of the entire system. As such, mesh division significantly influences both the computational accuracy and the resource demands of the simulation. To assess the impact of mesh density, simulations were carried out using mesh counts of 18990, 50510, and 212776. The resulting error remained below 0.39% across these cases, indicating convergence. Although finer meshes can further enhance accuracy, they also substantially increase computational cost and time. Therefore, a mesh size of 50510 elements was selected as an optimal balance between accuracy and efficiency for the simulations presented in this study.

## 3. Results and discussion

Figures 4(a) and 4(b) present the absorption and scattering cross sections for single Si nanoparticles and Si–12Au hybrid nanoparticles. As shown, a single Si nanoparticle exhibits absorption peaks at wavelengths of 430 nm and 525 nm. In contrast, the Si–12Au hybrid nanoparticles also display two absorption peaks: one at 430 nm, similar to that of the pure Si nanoparticle, and another at a longer wavelength of 545 nm. Compared to the pure Si particles, the second absorption peak of the hybrid structure is red-shifted, which is attributed to the doping effect that alters the electronic structure and narrows the bandgap, resulting in the observed redshift. The peak absorption cross section of Si at $\lambda = 430$ nm is 24623 nm$^2$, while that of the Si–12Au hybrid nanoparticles at $\lambda = 545$ nm reaches 39354 nm$^2$. In terms of scattering, the maximum scattering cross section of Si is 31907 nm$^2$, significantly larger than that of the hybrid nanoparticles.

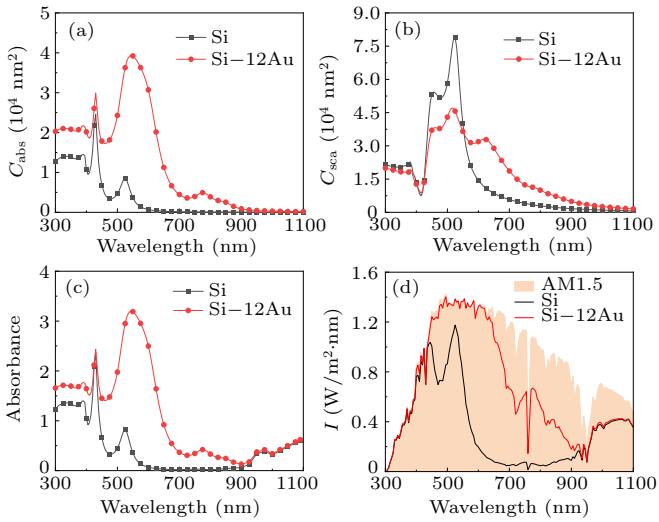



**Fig. 4.** (a) Absorption cross section, (b) scattering cross section, (c) absorbance, and (d) solar absorption spectrum at a volume fraction $f_{\mathrm{v}} = 10$ ppm and an optical path length $h = 20$ mm.

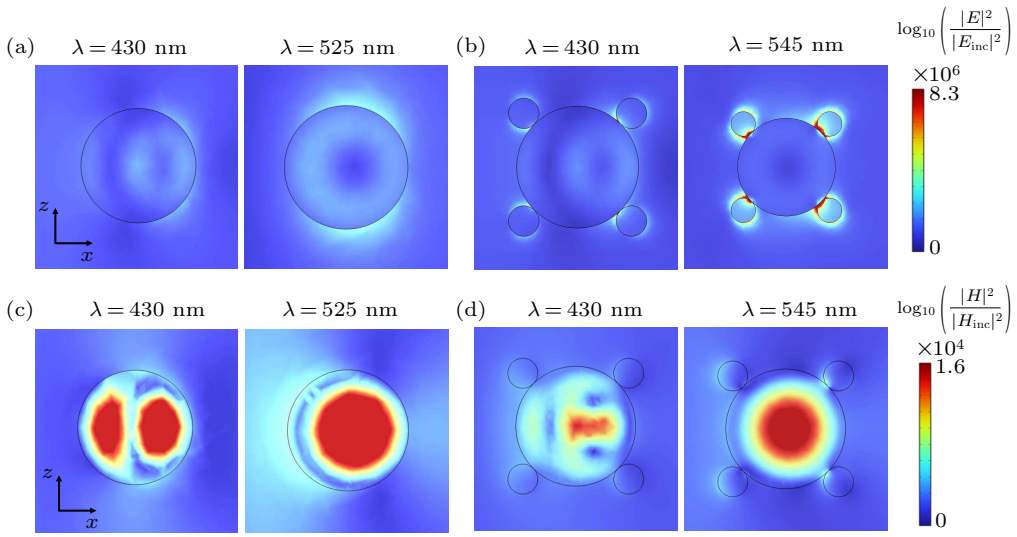



**Fig. 5.** Electric field distribution of (a) the Si nanoparticle at 430 nm and 525 nm, and (b) the Si–12Au hybrid nanoparticle at 430 nm and 545 nm. Magnetic field distribution of (c) the Si nanoparticle at 430 nm and 525 nm, and (d) the Si–12Au hybrid nanoparticle at 430 nm and 545 nm.

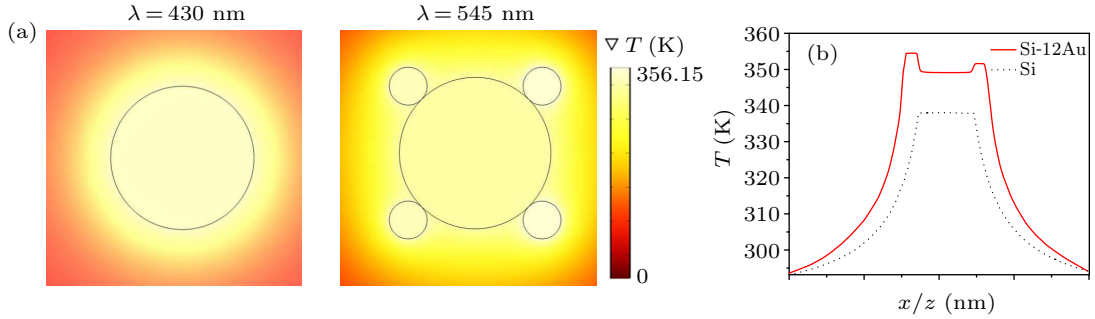



**Fig. 6.** (a) Maximum temperature distribution, and (b) temperature profile along the 3D cross-sectional line of Si at $\lambda = 430$ nm and Si–12Au hybrid nanoparticles at $\lambda = 545$ nm.

Figure 4(c) illustrates the simulated absorbance of different nanofluids (at a volume fraction of 10 ppm and an optical path length of 20 mm). According to the Beer–Lambert law, the maximum absorbance of the Si–12Au hybrid nanofluid exceeds that of the pure Si nanofluid by approximately 0.8 under identical conditions. As depicted in Fig. 4(d), the absorption characteristics under the AM 1.5 solar radiation spectrum are shown. The absorption spectrum of the Si–12Au hybrid nanofluid closely matches the solar spectrum. In particular, in the wavelength range of 400 nm to 920 nm, the hybrid nanoparticles demonstrate superior absorption capabilities compared to pure Si. When evaluating photothermal conversion efficiencies, conventional Si shows an efficiency of 38%, while the hybrid nanoparticles achieve 76%.

Figure 5 illustrates the electric and magnetic field distributions for both Si nanoparticles and Si–12Au hybrid nanoparticles at various absorption peaks. When Au nanoparticles are attached to the Si surface, the interaction with incident light excites LSPR in the Au particles. This LSPR effect significantly enhances the electric field on the surfaces of the Au nanoparticles, especially at the Si–Au interface, where strong electromagnetic activity is observed. Since silicon is a semiconductor, its quadrupolar resonance response couples with the surface electric field of the Au particles, forming localized regions of enhanced electric fields.[49] Similar to the electric field distribution, the LSPR in Au nanoparticles also influences the surrounding magnetic field, especially near the edges and surfaces of the particles, where localized magnetic field variations occur. Furthermore, the uniform distribution of Au nanoparticles contributes to a more consistent magnetic field within the silicon matrix.

The analysis focuses on the maximum attainable temperature of Si and Si–12Au hybrid nanoparticles dispersed in an aqueous solution. As illustrated in Fig. 6(a), the temperature field distributions at wavelengths of $\lambda = 430$ nm and $\lambda = 545$ nm are presented. The results indicate that the temperature of the hybrid nanoparticles and their surrounding aqueous environment is significantly higher than that of the pure Si nanofluid. Moreover, the hybrid nanoparticles are capable of heating a larger volume of the solution.

This enhanced heating effect is primarily attributed to the LSPR, which leads to a substantial amplification of the electric field near the surface of the Au nanoparticles.[50] The intensified electric field enhances light absorption, and the absorbed energy is subsequently converted into thermal energy, resulting in a temperature rise. Additionally, due to the high

thermal conductivity of Au, both the nanoparticle surface and the adjacent solution experience a gradual increase in temperature. In contrast, Si exhibits relatively lower thermal conductivity, which may cause heat accumulation near its surface. These combined effects contribute to a higher local temperature around the Au nanoparticles.

A cross-sectional temperature profile at the plane $x = z$ is shown in Fig. 6(b), and it corroborates the spatial trends observed in the temperature field. Since the incident light is directed along the positive $x$-axis, the Au nanoparticle located at the leftmost position experiences the highest temperature, reaching 354.5 K. The temperature variation within the Si core is relatively small; however, the integration of Au nanoparticles increases the overall temperature by approximately 11 K.

The optical absorption characteristics and photothermal conversion efficiency of Si–12Au hybrid nanoparticles were analyzed with respect to size parameters. Figure 7 presents the absorption efficiency, scattering efficiency, absorption spectrum, and photothermal conversion efficiency for different Si radii ($R = 30$ nm, 60 nm, and 90 nm). The analysis reveals a clear trend: as the particle size increases, the first absorption peak undergoes a significant red shift, indicating that larger particles tend to absorb light at longer wavelengths compared to smaller ones. In contrast, the second absorption peak remains relatively unaffected by changes in particle size.

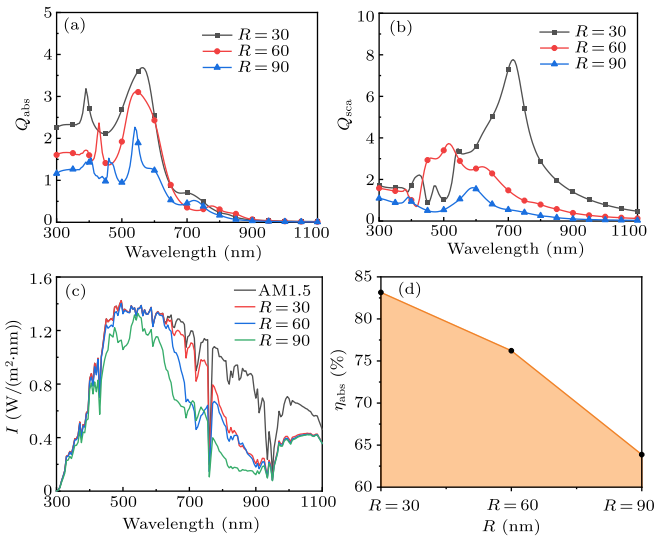



**Fig. 7.** (a) Absorption efficiency, (b) scattering efficiency, (c) absorption spectrum, and (d) photothermal conversion efficiency for different Si radii.

However, the scattering efficiency exhibits a notable variation when the Si sphere has a radius of $R = 30$ nm. This behavior may be attributed to the Au nanoparticles having a radius of $r = 15$ nm; with multiple Au particles attached, the internal Si surface receives less direct incident light, resulting in stronger scattering dominated by the external Au nanoparticles. As shown in Fig. 7(c), reducing the size of Si particles brings their absorption spectrum closer to the solar spectrum. Correspondingly, the photothermal conversion efficiency decreases with increasing Si radius, with values of 83.15%, 76.22%, and 63.87% for $R = 30$ nm, 60 nm, and 90 nm, respectively.

Figure 8 depicts the absorption efficiency, scattering efficiency, absorption spectrum, and photothermal conversion efficiency for different Au nanoparticle radii ($r = 15$ nm, 20 nm, and 25 nm). The figure clearly shows that as the radius of the Au sphere increases, the second absorption peak undergoes a noticeable redshift, while the first absorption peak remains largely unaffected.

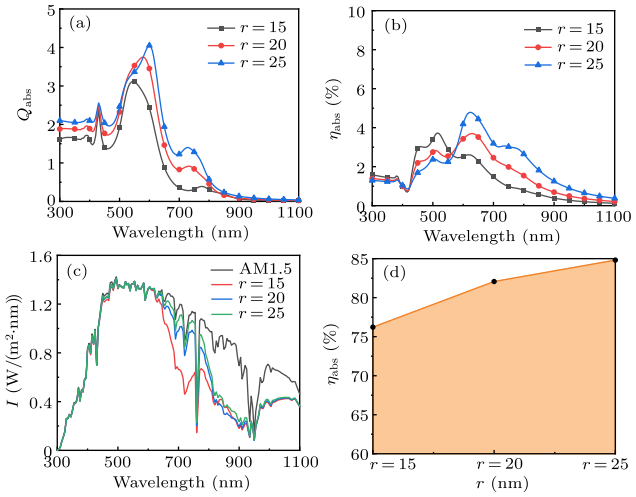



**Fig. 8.** (a) Absorption efficiency, (b) scattering efficiency, (c) absorption spectrum, and (d) photothermal conversion efficiency for different Au radii.

However, the scattering efficiency exhibits a significant change at $\lambda = 560$ nm for the Si spheres. This is attributed to the fact that the LSPR intensifies when the wavelength of the incident light more closely matches the collective oscillation frequency of the particles' electrons, leading to increased scattering intensity.

As shown in Fig. 8(c), with increasing Au particle size, the absorption spectrum aligns more closely with the solar spectrum. The photothermal conversion efficiency exhibits a positive correlation with the Au radius, although the rate of increase diminishes. Specifically, at $r = 20$ nm, the efficiency increases by 5.85% compared to $r = 15$ nm, while at $r = 25$ nm, the increase is only 2.74% compared to $r = 20$ nm.

## 4. Conclusion

In summary, this study investigates the structural characteristics and photothermal properties of dielectric nanoparticles combined with plasmonic nanoparticles by constructing Si–12Au hybrid nanoparticles and performing numerical simulations. A comparative analysis of the optical properties, temperature variations, and photothermal conversion efficiency was conducted between Si nanoparticles and the hybrid nanoparticles.

The results demonstrate that, compared to pure Si nanoparticles, the Si–12Au hybrid nanoparticles exhibit a redshift in the absorption peak along with a broader resonance band. The plasmonic resonance of Au nanoparticles coupled with the quadrupole resonance of Si nanoparticles leads to an enhanced electric field in the hybrid structure, resulting in a temperature increase with a maximum value of 354.5 K. The effects of varying the radii of Si and Au nanoparticles on the hybrid nanoparticles' performance were also examined. The findings reveal a distinct trend in photothermal conversion efficiency with respect to the Si nanoparticle radius. Specifically, at a concentration of 10 ppm and an optical path length of 20 mm, the efficiency decreases as the Si radius increases, with values of 83.15%, 76.22%, and 63.87% for radii of 30 nm, 60 nm, and 90 nm, respectively. Conversely, the photothermal conversion efficiency increases with the Au nanoparticle radius, although the rate of increase diminishes, showing increments of 5.85% and 2.74% between the sizes studied. This research provides theoretical insights into the design and application of hybrid nanostructures composed of dielectric and plasmonic nanoparticles for enhanced photothermal applications.

## Acknowledgements

This work is supported by the National Natural Science Foundation of China (Grant No. 52106099) and the Taishan Scholars Program of Shandong.

## References

[1] Kuznetsov A I, Miroshnichenko A E, Brongersma M L, Kivshar Y S and Luk'yanchuk B 2016 *Science* **354** 2472
[2] Jahani S and Jacob Z 2016 *Nat. Nanotechnol.* **11** 23
[3] Zograf G P, Petrov M I, Makarov S V and Kivshar Y S 2021 *Adv. Opt. Photon.* **13** 643
[4] Länk N O, Johansson P and Käll M 2020 *ACS Photonics* **7** 2405
[5] Li Y Q, Yang X Y, Yang Y J, Wang B B, Li X Y and Salas-Montiel R 2019 *Opt. Express* **27** 30971
[6] Jaque D, Maestro L M, Rosal B D, Gonzalez P H, Benayas A and Plaza J L 2014 *Nanoscale* **6** 9494
[7] Tran V A, Lee S W, Phan T T T, Don T N, Vien V, Thanh N C, Ho N N, Doan V D and Le V T 2024 *Mater. Today Chem.* **40** 102272
[8] Shridharan T S, Sivanantham A, Lee J H, Hong S Y, Jeong Y J, Shin S S and Cho I S 2024 *Chem. Eng. J.* **486** 150247
[9] Trinh P V, Anh N N, Cham N T, Tu L T, Hao N V, Thang B H, Chuc N V, Thanh C T, Minh P N and Fukata N 2022 *RSC Adv.* **12** 10514
[10] Li H, Yang S, Hu J, Zhang Z, Tang P, Jiang Y, Tang L and Zou B 2022 *Mater. Sci. Semicond. Process.* **146** 106661
[11] Bubnov A A, Syui A V, Popov A A, Tikhonovskii G V, Pokryshkin N S and Timoshenko V Y 2023 *Phys. At. Nucl.* **86** 2743
[12] Vikram M P, Nishida K, Li C H, Riabov D, Pashina O and Tang Y L 2024 *Nanophotonics* **13** 21928606
[13] Chen T S, Gao J Y, Wang X X, Chen Y Z, Yang H and Qi Y P 2025 *Phys. Scr.* **100** 015533
[14] Rao X J, Zhu H R, Wang X X, Chen Y Z, Qi Y P and Yang H 2025 *J. Opt. Soc. Am. B* **42** 431
[15] Zograf G P, Petrov M I, Zuev D A, Dmitriev P A, Milichko V A, Makarov S V and Belov P A 2017 *Nano Lett.* **17** 2945
[16] Amjad M, Jin H, Du X and Wen D 2018 *Sol. Energy Mater. Sol. Cells* **182** 255
[17] Gu P, Yang H J, Li D Q, Zhu H Q, Chen J, Zhang Z X, Yan Z D, Tang C J, Liu F X, Chen Z and Zhang Z X 2024 *J. Phys. Chem. C* **128** 6431
[18] Zhu X, Zhang J Y, Yang C H, Li Y and Chen Y Y 2023 *Chin. Phys. Lett.* **40** 057801
[19] Yan G D, Zhang Z H, Guo H, Chen J P, Jiang Q S, Cui Q N, Shi Z L and Xu C X 2023 *Chin. Phys. B* **32** 067302
[20] Li X M, Liu F M, Li Z G, Zhu H Y, Wang F and Zhong X L 2023 *Chin. Phys. B* **32** 114205
[21] Chen X W, Qin C Y, Yang L, Li X K, Wu X H and Zhang B 2024 *Int. J. Therm. Sci.* **200** 108980
[22] Zou Y, Qin C Y, Zhai H, Sun C L, Zhang B and Wu X H 2022 *Int. J. Therm. Sci.* **182** 107824
[23] Landfester K 2009 *Angew. Chem. Int. Ed.* **48** 4488
[24] Vallejo J P, Prado J I and Lugo L 2022 *Appl. Therm. Eng.* **203** 117926
[25] Sathish T, Giri J, Saravanan R, Ubaidullah M, Shangdiar S, Iikela S, Sithole T and Amesho K T T 2024 *Appl. Therm. Eng.* **252** 123692
[26] Zhou K, Jee S W, Guo Z, Liu S and Lee J H 2011 *Appl. Opt.* **50** 63
[27] Ge W, Zhang X R, Liu M, Lei Z W and Lu Y L 2015 *Mater. Res. Innov.* **18** 701
[28] Gerasimova E N, Uvarov E, Yaroshenko V V, Epifanovskaya O, Shakirova A, Logunov L S, Vlasova O, Parodi A, Zamyatnin A A Jr., Timin A S, Makarov S V and Zyuzin M V 2023 *ACS Appl. Nano Mater.* **6** 18848
[29] Gurbatov S O, Puzikov V, Cherepakhin A, Mitsai E, Tarasenka N, Shevlyagin A, Sergeev A, Kulinich S A and Kuchmizhak A A 2022 *Opt. Laser Technol.* **147** 107666
[30] Cortie M B and McDonagh A M 2011 *Chem. Rev.* **111** 3713
[31] Chehaidar A 2023 *Int. J. Therm. Sci.* **188** 108227
[32] Yu X, Fan S L, Zhu B, El-Hout S I, Zhang J and Chen C L 2025 *Green Energy Environ.* **10** 1377
[33] Gupta A, Ghosh S, Thakur M K, Zhou J, Ostrikov K K, Jin D and Chattopadhyay S 2021 *Prog. Mater. Sci.* **121** 100838
[34] Sun C L, Zou Y, Qin C Y, Chen M J, Li X K, Zhang B and Wu X H 2022 *Renew. Energy* **189** 402
[35] Yang Q H, Qin C Y, Chen N, Liu H T, Zhang B and Wu X H 2024 *Int. J. Therm. Sci.* **204** 109175
[36] Wu Y X, He Q, Zhang H, Meng X L, Min Y Y, Wang Y, Wu X H, Zhang P, Ma Y Y and Zheng Y Q 2025 *J. Mater. Chem. C* **13** 5370
[37] Green M A 2008 *Sol. Energy Mater. Sol. Cells* **92** 1305
[38] Rakić A D, Djurišic A B, Elazar J M and Majewski M L 1998 *Appl. Opt.* **37** 5271
[39] Farooq S, Rativa D, Said Z and de Araujo R E 2023 *Appl. Therm. Eng.* **218** 119212
[40] Yang Q H, Qin C Y, Zou Y, Liu H T, Zhang B and Wu X H 2023 *Int. J. Therm. Sci.* **191** 108387
[41] Wang X J, Wang Y Q, Yang X X and Cao Y 2019 *Sol. Energy* **181** 439
[42] Zhao J, Pinchuk A O, Mcmahon J M, Li S Z, Ausman L K, Atkinson A L and Schatz G C 2008 *Acc. Chem. Res.* **4** 1710
[43] Sun C L, Qin C Y, Zhai H, Zhang B and Wu X H 2021 *Nanomaterials* **11** 2722
[44] Chen M J, Wang X, Hu Y and He Y 2020 *J. Quant. Spectrosc. Radiat. Transf.* **250** 107029
[45] Khademalrasool M and Talebzadeh M D 2021 *Adv. Powder Technol.* **32** 2916
[46] Zeng J and Xuan Y 2021 *J. Quant. Spectrosc. Radiat. Transf.* **269** 107692
[47] Chen M J, He Y R, Huang J and Zhu J Q 2017 *Int. J. Heat Mass Transf.* **108** 1894
[48] Zou Y, Yang L, Li X K, Qin C Y, Zhang B and Wu X H 2024 *Heat Transf. Eng.* **1** 12
[49] Kucherik A, Kutrovskaya S, Osipov A, Gerke M, Chestnov I, Arakelian S, Shalin A S, Evlyukhin A B and Kavokin A V 2019 *Sci. Rep.* **9** 338
[50] Wang Q R, Yang L, Zhao N, Xu G Y, Song J Z, Jin X, Li X and Liu S H 2023 *Appl. Therm. Eng.* **219** 119476